

# Chicken meat and bone meal valorization by hydrothermal treatment and anaerobic digestion: Biofuel production and nutrient recovery

A. Sarrion<sup>a,\*</sup>, R.P. Ipiales<sup>a,b</sup>, M.A. de la Rubia<sup>a</sup>, A.F. Mohedano<sup>a</sup>, E. Diaz<sup>a</sup>

<sup>a</sup> Engineering Department, Universidad Autónoma de Madrid, 28049, Madrid, Spain

<sup>b</sup> Arquimea, 28400, Collado Villalba, Madrid, Spain

## ARTICLE INFO

### Keywords:

Anaerobic digestion  
Chicken meat and bones meal  
Circular economy  
Energy recovery  
Hydrothermal treatment  
Struvite

## ABSTRACT

In this work, chicken meat and bones (C-MBM) waste is treated through a sequence of stages including hydrothermal treatment (HTT), nutrient recovery and anaerobic digestion, with the aim of evaluating their potential synergy as a circular economy approach. HTT was carried out at 170, 200 and 230 °C, under non-acidic and acidic conditions using 0.5 M HCl (HTT-A). Phosphorous from process water was recovered by chemical precipitation with the addition of a Mg salt, and the liquid effluent was anaerobically treated to degrade organic matter and produce a methane-rich biogas. Hydrochar obtained under non-acidic conditions presented poor combustion characteristics, while HTT-A yielded a bio-oil with high higher heating value ( $\approx 38$  MJ/kg), good combustibility performance and high reactivity. More than 95% phosphorous (as phosphate) and almost 100% nitrogen (being 30% as  $\text{NH}_4\text{-N}$ ) content in C-MBM were solubilized in the process water upon HTT-A, while these nutrients were mainly retained in the hydrochar in non-acidic reactions. Chemical precipitation of P and  $\text{NH}_4\text{-N}$  from HTT-A process water allowed recovering a crystalline solid identified as struvite and a struvite-apatite mixture, with negligible heavy metals content. High methane production (250–300 mL  $\text{CH}_4/\text{g COD}_{\text{added}}$ ) and organic matter removal (up to 75%) were achieved in the anaerobic tests. HTT proves to be a suitable treatment for material and energetic valorization of C-MBM, within a circular economy framework, which allows to obtain high value-added products (hydrochar/bio-oil, biofertilizers and biogas).

## 1. Introduction

Chicken meat and bones meal (C-MBM) is a waste produced from poultry slaughterhouse or rendering industries consisting in a mixture of small pieces of bones, fat, and residual fractions of meat. Meat and bones meal (MBM) is widely used as a low-cost pet food formulation, because of their high protein content, but the nutritional properties vary dramatically, and in some cases, further processing is required [1]. Although MBM can be seen as a waste from the slaughterhouse operations, this material become much more valuable after processing. In this way, MBM as feedstock for anaerobic digestion (AD) [2,3] or co-incineration in cements kilns [4] allows energy recovery.

Anaerobic digestion of MBM is an attractive alternative with high methane production  $\approx 340$  mL  $\text{CH}_4$  per gram of volatile solids and a large organic matter removal 40–75% [3,5], while up to 40% of the coal can be replaced by MBM in cement kilns [6]. However, the presence of a high amount of solids (specially bones), high protein and fat content, produce several issues such as longer periods of time to degrade the

feedstock, ammonia oversaturation and inhibition during AD [3,7]. Diversely, the large energy demands for MBM drying and grinding, as well as the large amount of residual ash in incineration led to an excessive amount of ash in chambers that could produce ash agglomeration, corrosion, fouling and energy deficiency in combustion systems [8,9].

MBM is generally rich in nutrients, specially phosphorus, which is a scarce mineral used as fertilizer [10]. Phosphorus is an essential nutrient to keep the agricultural yields and was added to the list of the “20 Critical Raw Materials” in 2014 [11]. According to Leng et al. [12], up to 25 kg of P could be recovered by ton of MBM. In the European Union more than 13 Mt of MBM was produced in 2020 [13], considering above assumption, MBM could represented up to 156,000 ton of P per year ( $\approx 12\%$  of the total phosphorus consumption in the European Union) [14]. The bones contain up to 15% of phosphorus (as hydroxyapatite and ossein-apatite) in dry weight [15].

A possible way to complete valorization (energy and nutrient recovery) of MBM could be achieved by hydrothermal treatment (HTT).

\* Corresponding author.

E-mail address: [andres.sarrion@uam.es](mailto:andres.sarrion@uam.es) (A. Sarrion).

<https://doi.org/10.1016/j.renene.2023.01.005>

Received 31 October 2022; Received in revised form 2 December 2022; Accepted 3 January 2023

Available online 3 January 2023

0960-1481/© 2023 The Authors. Published by Elsevier Ltd. This is an open access article under the CC BY-NC-ND license (<http://creativecommons.org/licenses/by-nc-nd/4.0/>).

Under hydrothermal carbonization conditions (170–250 °C, and self-generated pressure), wide range of wet biomass waste, are chemically transformed, promoting its dehydration and decarboxylation [16]. This process generates a carbon-rich solid called hydrochar with high carbon content and higher heating value (HHV) [17], and a liquid fraction, so-called process water, with high organic matter, nutrients, and mineral content [18], which can be valorized to obtain biofertilizers and biogas through chemical precipitation and AD, respectively [16].

Hydrochar is mainly used as a solid biofuel [19] because of its improved properties compared to raw biomass, but it has also been successfully used in several environmental applications such as soil amendment [20], energy storage [21], activated carbon precursor [22], and catalyst support [23]. On other hand, process water represents a potential source of nutrients (mainly N and P) [24] and energy recovery through chemical precipitation and AD, respectively [25]. However, conventional HTT retained most of the P (~85%) and other nutrients (K, Mg, Ca) in the hydrochar structure [26]. In this way, acid-assisted HTT (HTT-A) has appeared as an effective technique which improves the solubilization of mineral and heavy metals, and nutrients to process water (above 90% P and N) improving waste carbonization and reducing the ash content in the hydrochar [27].

This work focuses on studying C-MBM management by HTT and acid-assisted HTT at temperatures in the range of 170–230 °C with the aim to obtain, in a first stage, a hydrochar and/or a bio-oil to be used as biofuel, according to their energetic characteristics and combustion properties. The valorization of process water to recover nutrients by precipitation of  $\text{PO}_4\text{-P}$  and  $\text{NH}_4\text{-N}$  as struvite, and the anaerobic treatment of the liquid effluent to remove organic matter and produce a methane-rich biogas within a circular economy framework are also studied. So far, there is not a comprehensive study on the integration of hydrothermal treatment for the management of C-MBM, together with a material recovery stage (nutrients) and anaerobic digestion of the process water for a complete valorization of this waste.

## 2. Materials and methods

### 2.1. Chicken meat and bones meal

The C-MBM was collected from a butcher shop (Madrid, Spain), grounded with an industrial mixer MP350 and frozen at  $-20\text{ }^{\circ}\text{C}$  to facilitate its preservation. The C-MBM presented the following main characteristics:  $66.0 \pm 2.1$  wt% moisture,  $\text{pH } 6.3 \pm 0.5$ , measured with a Mettler-Toledo InLab Solids Pro-ISM pH-meter,  $258.5 \pm 1.2$  g  $\text{O}_2/\text{L}$  total chemical oxygen demand (TCOD),  $665.2 \pm 2.3$  g/L total solid (TS),  $523.5 \pm 1.4$  g/L volatile solid (VS),  $8.1 \pm 0.6$  g/L total Kjeldahl nitrogen (TKN),  $26.9 \pm 0.2$  g  $\text{PO}_4\text{-P}/\text{kg}$ ,  $39.1 \pm 0.2$  g  $\text{Ca}/\text{kg}$  and  $4.9 \pm 0.2$  g  $\text{K}/\text{kg}$ .

### 2.2. Hydrothermal experiments

Hydrothermal treatment was carried out in an electrically heated ZipperClave pressure vessel (4 L) with heating ramp of  $3\text{ }^{\circ}\text{C}/\text{min}$  under non-acidic or acidic conditions. In each experiment, the reactor was loaded with 1.5 kg C-MBM (90 wt% moisture) by addition of deionized water and heated at  $170\text{ }^{\circ}\text{C}$ ,  $200\text{ }^{\circ}\text{C}$  and  $230\text{ }^{\circ}\text{C}$  for 1 h. Acid-assisted HTT was carried out under 0.5 M HCl conditions (initial  $\text{pH} \sim 4$ ), considering both the moisture of the feedstock and the added water to assure hydrothermal conditions in the reactor. The reaction was stopped by cooling with an internal heat exchanger using tap water. Conventional HTT products (hydrochar and process water) were separated by filtration with a  $250\text{ }\mu\text{m}$  membrane vacuum filter. The acid-assisted HTT product, a mixture of bio-oil (BiO-A) and process water, was separated by centrifugation (Orto Alresa centrifuge) at 8000 rpm for 10 min, and the supernatant was filtered through a  $250\text{ }\mu\text{m}$  filter. The HTT products

were labeled as HC (hydrochar), and PW (process water) followed by the HTT temperature (i.e., HC170 or PW170, referred to the hydrochar and process water obtained in HTT at  $170\text{ }^{\circ}\text{C}$  for 1 h). After acid-assisted HTT, a bio-oil product was obtained instead of hydrochar, and it was labeled as BiO. In the case of acid-assisted HTT, the letter A, specifying acid addition, was added to BiO and PW, both followed by the HTT temperature (i.e., BiO170-A and PW170-A). The yield of the HTT products was calculated by the following equations. The yield of the HTT products was calculated by the following equations. Hydrochar mass yield ( $Y_{\text{HC}}$ ), i.e., the weight ratio of hydrochar recovered ( $W_{\text{HC}}$ ) to C-MBM feedstock ( $W_{\text{C-MBM}}$ ) on a dry basis, was calculated with (Eq. (1)):

$$Y_{\text{HC}} (\text{wt.}\%) = \frac{W_{\text{HC}}}{W_{\text{C-MBM}}} \cdot 100 \quad (1)$$

Likewise, bio-oil mass yield ( $Y_{\text{BiO-A}}$ ), is the weight ratio of bio-oil recovered ( $W_{\text{BiO-A}}$ ) to C-MBM ( $W_{\text{C-MBM}}$ ) on a dry basis, and was calculated with (Eq. (2)):

$$Y_{\text{BiO-A}} (\text{wt.}\%) = \frac{W_{\text{BiO-A}}}{W_{\text{C-MBM}}} \cdot 100 \quad (2)$$

The yield of process water ( $Y_{\text{PW}}$ ) was calculated as TS present in PW ( $W_{\text{PW-TS}}$ ) to C-MBM ( $W_{\text{C-MBM}}$ ) ratio on a dry basis (Eq. (3)):

$$Y_{\text{PW}} (\text{wt.}\%) = \frac{W_{\text{PW-TS}}}{W_{\text{C-MBM}}} \cdot 100 \quad (3)$$

### 2.3. Nutrient recovery stage

A magnesium agent ( $\text{Mg}(\text{OH})_2$ ) was added to a sample of 50 mL of process water or acid process water (process water from HTT-A) to promote the struvite formation according to molar ratio of  $\text{NH}_4\text{:Mg:PO}_4$  to 1:1.3:1 [28]. The mixture was neutralized with 2 M NaOH to  $\text{pH } 9$  and maintained under stirring for 20 min. The precipitated solid was separated by filtration through  $0.45\text{ }\mu\text{m}$  and dried by oven at  $105\text{ }^{\circ}\text{C}$  during 24 h. The solid recovered were labeled as ST (in terms of struvite) followed to the HTT operating conditions (i.e., ST170 or ST170-A). The liquid effluent resulting of the nutrients recovery stage was labeled as secondary process water PW-S, or PW-A-S.

### 2.4. Anaerobic digestion experiments

Anaerobic digestion runs were carried out in 120 mL glass serum vials, filled with 60 mL suspension of process water, inoculum, substrate, deionized water and a basal medium with macro- and micro-nutrients [29]. Granular anaerobic sludge, from a brewery wastewater treatment plant (operating at  $35\text{ }^{\circ}\text{C}$ ), was used as inoculum with the following characteristics:  $53.7 \pm 0.9$  g TS/L,  $46.2 \pm 0.9$  g VS/L and a TCOD of  $33.1 \pm 2.0$  g  $\text{O}_2/\text{L}$ . The initial inoculum concentration was set at 15 g VS/L and the inoculum-to-substrate ratio at 2 on a COD basis for all runs. The vials were sealed with rubber stops and metal crimps and were flushed with  $\text{N}_2$  for 3 min to ensure anaerobic conditions. The vials were kept under mesophilic conditions ( $35 \pm 1\text{ }^{\circ}\text{C}$ ) in a thermostatic shaking water bath at 100 rpm. AD was monitored using 10 vials for each run: three for biogas measurements (volume and composition), and the other seven were sacrificed during the experiment to monitor parameters such as pH, soluble COD (SCOD), alkalinity, total volatile fatty acid (TVFA) and ammoniacal nitrogen. Triplicate blank samples with no substrate were run to determine the background methane yield of the inoculum, and triplicate control experiments were also performed with starch to check inoculum activity. Methane yield was calculated by subtracting the amount of methane produced by blanks, and methane volume at standard temperature and pressure (STP;  $0\text{ }^{\circ}\text{C}$ , 1 atm) was recorded.

**Table 1**

Characteristics and combustion kinetic properties of C-MBM, hydrochars, and bio-oils (d.b.).

	C-MBM	HC170	HC200	HC230	BiO170-A	BiO200-A	BiO230-A
Yield (%)	–	33.3 ± 0.3	31.3 ± 0.7	20.7 ± 1.2	9.2 ± 1.0	8.6 ± 1.2	8.5 ± 0.9
C (%)	53.7 ± 0.8	28.1 ± 1.5	23.5 ± 0.1	41.7 ± 0.4	74.9 ± 0.0	75.1 ± 0.0	75.3 ± 0.1
H (%)	7.5 ± 0.1	4.1 ± 0.2	2.2 ± 0.0	3.7 ± 0.1	11.1 ± 0.0	11.2 ± 0.0	11.2 ± 0.1
N (%)	7.8 ± 0.2	2.3 ± 0.0	1.5 ± 0.1	1.5 ± 0.0	0.3 ± 0.0	0.3 ± 0.0	0.5 ± 0.0
S (%)	0.5 ± 0.0	0.2 ± 0.0	0.1 ± 0.0	0.1 ± 0.0	0.1 ± 0.0	0.1 ± 0.0	0.1 ± 0.0
O <sup>a</sup> (%)	17.8 ± 0.1	24.7 ± 0.2	26.5 ± 0.0	12.7 ± 0.1	13.4 ± 0.0	13.0 ± 0.0	12.6 ± 0.0
HHV (MJ/kg)	25.4 ± 0.1	10.9 ± 0.1	11.6 ± 0.0	19.8 ± 0.0	37.9 ± 0.0	38.1 ± 0.0	38.2 ± 0.0
VM (%)	86.2 ± 0.6	59.0 ± 1.2	52.3 ± 0.4	55.3 ± 0.3	98.9 ± 0.1	98.5 ± 0.1	98.8 ± 0.1
FC (%)	1.0 ± 0.3	0.4 ± 0.2	1.5 ± 0.1	4.4 ± 0.2	0.9 ± 0.0	1.2 ± 0.0	1.0 ± 0.0
Ash (%)	12.8 ± 0.2	40.6 ± 0.3	46.3 ± 0.3	40.3 ± 0.2	0.2 ± 12.3	0.3 ± 12.3	0.2 ± 12.3
P (%)	26.8 ± 0.1	7.1 ± 0.1	7.3 ± 0.0	10.9 ± 0.1	4.1 ± 0.1	0.1 ± 0.0	9.2 ± 0.0
T <sub>i</sub> (°C)	249	280	300	302	236	239	212
T <sub>m</sub> (°C)	369	336	322	398	409	405	379
T <sub>b</sub> (°C)	725	654	582	520	486	492	485
CCI·10 <sup>7</sup> (min <sup>-2</sup> ·°C <sup>-3</sup> )	6.6	4.4	2.20	5.60	16.6	22.10	32.10
E <sub>a</sub> (kJ/mol)	41.6	39.8	41.8	29.4	16.4	19.6	11.4
Energy density	–	0.43	0.46	0.78	1.49	1.50	1.50
Energy yield (%)	–	14.3	14.4	16.2	13.7	12.9	12.8

<sup>a</sup> Calculated from the mass balance: O = 100-C-H-N-S-ash.

## 2.5. Analytical methods

The elemental composition (C, H, N and S) of hydrochar, bio-oil, process water and P-rich precipitate was determined on a CHNS analyzer (LECO CHNS-932), while inorganic elements (mineral and heavy metals) composition was measured by inductively coupled optical emission spectroscopy (ICP-OES) on an Iris Intrepid II XDL instrument (ThermoFisher Scientific). Proximate analysis (moisture, fixed carbon (FC), volatile matter (VM) and ash content) was done by thermogravimetric analysis using a Discovery SDT thermogravimetric (TG 209, F3, Netzsch), according to ASTM methods D3173, D3174, and D3175, respectively [30]. The oxygen content was calculated by difference (100–C–H–N–S–ash (wt.%)). The HHV of the hydrochar and BiO-A was estimated by Eq. (4) [31], where the concentration of C, H, S, N, O and ash is expressed as wt.% on a dry basis. The energy density, ratio of the higher heating value of hydrochar (HHV<sub>HC</sub>) or bio-oil (HHV<sub>BiO-A</sub>) to that of the feedstock (HHV<sub>C-MBM</sub>), was calculated by equation (5). The energy yield (E<sub>yield</sub>) of hydrochar and bio-oil, was calculated using Eq. (6):

$$HHV \text{ (MJ/kg)} = 0.349 \cdot C + 1.033 \cdot H + 0.100 \cdot S - 0.103 \cdot O - 0.015 \cdot N - 0.021 \cdot \text{Ash} \quad (4)$$

$$\text{Energy density} = \frac{HHV_{HC/BiO-A}}{HHV_{C-MBM}} \quad (5)$$

$$E_{\text{yield}} (\%) = Y_{HC/BiO-A} \cdot \text{Energy density} \quad (6)$$

Crystal structure of solid obtained in the nutrient recovery stage was analyzed by total reflection X-ray fluorescence (TXRF) spectroscopy on an Extra-II Rich & Seifert spectrometer equipped with a Si–Li detector.

Process water (before and after nutrient recovery stage) was characterized by measuring TS and VS according to standard methods 2540B and 2540E APHA, respectively [32], and TCOD by the method described in Raposo et al. [33]. Sacrificed samples were filtered (0.45 µm) and analyzed to determine: pH (Crison 20 Basic pH meter), SCOD and TKN applying the standard method 5220D and 4500B, respectively [32]. Ammonia nitrogen (NH<sub>4</sub>–N) was determined by distillation and titration (method 4500C) [32]. NO<sub>2</sub>–N and NO<sub>3</sub>–N content was determined on a Dionex ICS-900 ion chromatograph with chemical suppression and fitted with a 4 × 250 mm Dionex IonPac AS22 column, using a mobile phase of 1 mL/min of 1.4/4.5 mM NaHCO<sub>3</sub> and Na<sub>2</sub>CO<sub>3</sub>, respectively. Phosphate was analyzed photometrically using a Hach Lange LCK350 cuvette test. Total organic carbon (TOC) was determined using an OI

Analytical TOC analyzer (model 1010, Texas, USA). Individual VFA concentration were identified by gas chromatography (GC) in a Varian 430-GC instrument as described on a study carried by de la Rubia et al. [34]. Biogas production was determined using a manometric method, measuring the pressure increase in each vial with an electronic pressure monitor (ifm, PN 7097) [35], and biogas composition was determined using a Thermo Fisher Trace 1300 GC equipped with a thermal conductivity detector (TCD) [34].

## 2.6. Thermogravimetric and differential thermogravimetric analysis

Thermogravimetric analysis (TG) and differential thermogravimetric (DTG) of hydrochar and BiO-A, were carried out by a Discovery SDT 650 thermogravimetric analyzer to determine ignition (T<sub>i</sub>), burnout (T<sub>b</sub>), and peak temperature of the maximum loss weight (T<sub>m</sub>), characteristic parameters of combustion reflecting the thermal behavior of fuels during the combustion process. In addition, the thermal analysis allowed the determination of kinetic parameters by Flynn-Wall-Ozawa (FWO) model [36], which describes the dependence of the activation energy (E<sub>a</sub>) and the degree of conversion during the combustion. Equations (6)–(8) describe the kinetic and combustion parameters:

$$\ln(\beta) = \ln\left(\frac{A \cdot E_a}{R \cdot g(\alpha)}\right) - 5.331 - 1.052 \cdot \frac{E_a}{R \cdot T} \quad (6a)$$

$$\alpha = \frac{m_0 - m_f}{m_0 - m_\infty} \quad (7)$$

where β is the heating rate, A is the frequency factor, E<sub>a</sub> is the activation energy, R is the universal gas constant (8.314 J/mol), g(α) is the conversion degree, T is the absolute temperature (K), m<sub>0</sub>, m<sub>f</sub> and m<sub>∞</sub> are the initial, current, and final weights of the samples, respectively. The values of E<sub>a</sub> can be determined from the slope of ln(β) against 1/T, while frequency factor is calculated from the intercept of this straight line [25].

The comprehensive combustion index (CCI) was calculated with (Eq. (8)) [25]:

$$CCI \text{ (min}^{-2} \cdot \text{°C}^{-3}) = \frac{DTG_m \cdot DTG_{\text{mean}}}{T_i^2 \cdot T_b} \quad (8)$$

where DTG<sub>m</sub> and DTG<sub>mean</sub> are the maximum and the average rate of weight loss, respectively, and T<sub>i</sub> and T<sub>b</sub> are the ignition and the burnout temperatures, respectively.

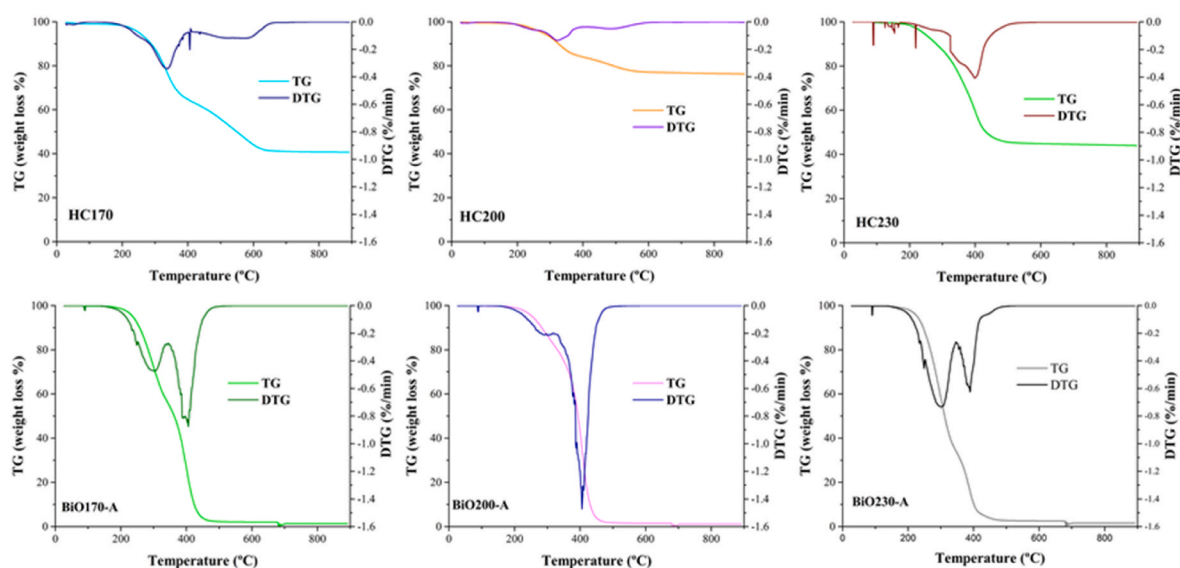


Fig. 1. Thermogravimetric and differential thermogravimetric profiles of hydrochars and bio-oils.

### 3. Results

#### 3.1. Characterization of feedstock, hydrochars and bio-oils

Table 1 summarizes the main characteristics of the feedstock, as well as hydrochar and bio-oil from HTT and HTT-A, respectively. The C-MBM was characterized by a high carbon ( $\approx 54\%$ ) and nitrogen ( $8\%$ ) content from animal protein and fat, and a moderate ash content ( $\approx 13\%$ ) mainly due to the calcium and phosphorus ( $\approx 50\%$ ) of the bones. In addition, C-MBM presented a significant HHV value ( $\approx 26$  MJ/kg) and a minimal FC content, mainly associated with the significant carbonate content of the bones [37]. The hydrochar showed a strongly drop up to  $50\%$  in average in carbon, nitrogen and HHV, while ash content increased by a 3-fold compared to C-MBM. HC230 showed a lower decrease in carbon content and HHV ( $\approx 20\%$  in both cases) regarding C-MBM, with similar ash content of the other hydrochars (HC170 and HC200). The sharp reduction of carbon and HHV in HC170 and HC200 was due to the high hydrolyzable compounds content such as carbohydrates, proteins and fatty acids [3,38], which were transferred to process water. This high content of hydrolyzable compounds resulted in low  $Y_{HC}$  value ( $21\text{--}33\%$ , being  $45\%$  ash) (see Table 1). However, the high  $Y_{HC}$ , carbon content and HHV in HC230 probably was due of most severe condition that contributed to the formation of secondary hydrochar, by polymerization, condensation, aromatization and Maillard reactions of soluble compounds in the process water that precipitate again in the hydrochar [39]. These results suggest high feedstock decomposition through

hydrolysis, dehydration, and decarboxylation reactions as temperature increases and an increase of the recombination of carbon-rich soluble compounds, which precipitate on the hydrochar, favoring carbon and energy densification as  $Y_{HC}$  decreases [40]. The mineral compounds forming the bone structure of C-MBM, such as carbonates, hydroxyapatite, osseine-apatite, lutein among others [41] were not affected by the hydrothermal treatment and remained in the hydrochar. The FC content remained almost constant, while the VM content was significantly reduced ( $32\text{--}40\%$ ), confirming the high solubilization of hydrolyzable organic compounds to the process water.

Acid-assisted HTT yielded a bio-oil (instead of the hydrochar) and a process water as HTT products. The bio-oil showed high carbon content ( $\approx 75\%$ ) and HHV ( $\approx 38$  MJ/kg), and low N, S, and ash content ( $<0.5\%$  in all cases). Considering the standard ISO/TS 17225-8 [42], which recommend a HHV  $>17$  MJ/kg,  $N < 3\%$ ,  $S < 0.5\%$ , ash  $<20\%$  and VM  $< 75\%$  for the use of biofuels from thermochemical process of biomass waste as alternative biofuel at industrial level, the hydrochar presented inadequate characteristics to be considered as biofuel because of the high ash content ( $\approx 40\%$ ) and low HHV (excepting HC230). Considering the energy density values, HC170 and HC200 would not be suitable for use as fuel because of their low energy density ( $<1$ ), indicating that the energy content of the hydrochar was lower than that of the feedstock. Otherwise, the bio-oil showed a suitable characteristic to be used as alternative biofuel at industrial level. However, the  $Y_{BIO-A}$  was lower than  $10\%$  in all cases, reaching poor energy recovery ( $E_{yield} < 15\%$ ), slightly lower than the energy recovery of the hydrochar  $\approx 25\%$ . These

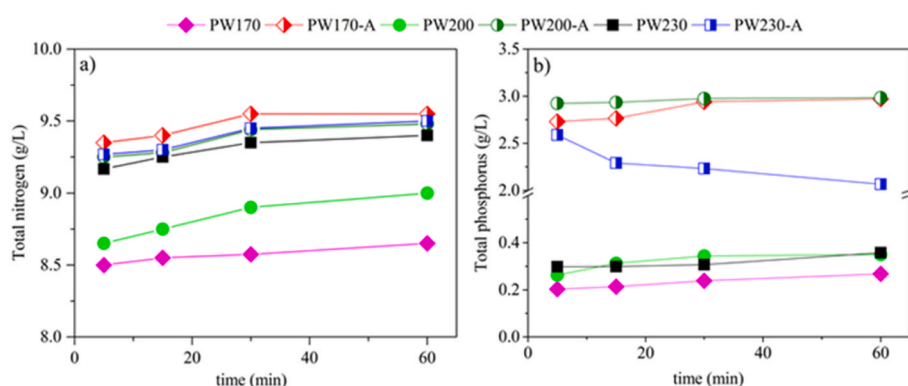


Fig. 2. Time course of nitrogen (a) and phosphorus (b) in process water from acid-free and acid-assisted HTT.



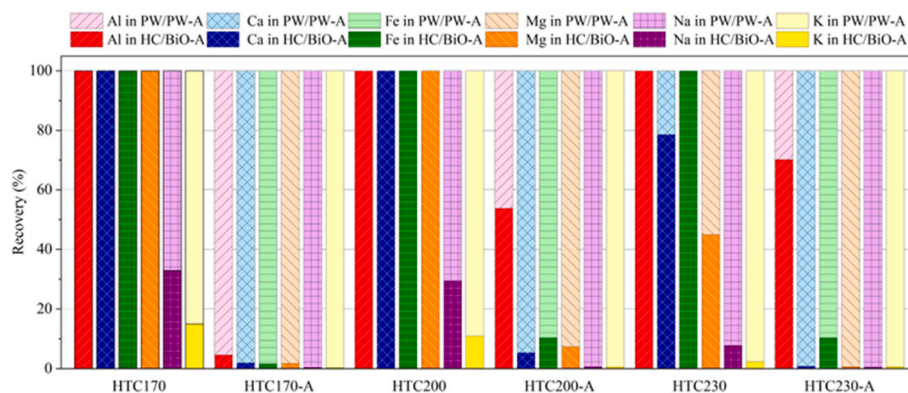


Fig. 3. Mineral distribution after 60 min reaction time for acid-free and acid-assisted HTT.

low energy yields, demand the valorization of process water by AD to improve the overall energy performance of the process.

Fig. 1 shows the TG and DTG data of hydrochar and bio-oil. TG and DTG combustion profiles of hydrochar and bio-oil showed different trends and combustion stages. Hydrochar presented a remarkable degradation between 280 and 400 °C with a weight loss up to 55 wt%, which is associated with the volatile matter of the hydrochars. A second stage between 500 and 600 °C was only evident for HC170, owing to combustion of FC and degradation of carbonates into CO<sub>2</sub> [43]. On other hand, TG and DTG profiles of bio-oils showed two different and marked zones of weight loss. These two degradation stages are probably related to the presence of compounds with different molecular weight and different ignition points [44,45]. In all cases, the bio-oil degradation was greater than 98 wt% during combustion.

The kinetic analysis from TG and DTG profiles shows that bio-oil displays higher CCI, and lower  $T_i$  and  $E_a$  than hydrochar (Table 1). Hydrochars and bio-oils showed a satisfactory combustion characteristic and turn both into a potential solid fuel. However, the better CCI and low  $T_i$  and  $E_a$  together with the high HHV and energy density, and low N, S, and ash content make to bio-oil a better and suitable fuel for industrial energy production than hydrochars. Despite of aforementioned, the low  $Y_{HC}$  and  $Y_{BiO-A}$  values suggest that these biofuels can be blended with mineral coals or hydrochars with elevated  $E_a$  and  $T_i$  [46].

### 3.2. Fate of nutrients, minerals, and organics

Fig. 2 shows the time course of nitrogen and phosphorus concentration into the process water during non-acidic and acid-assisted HTT. The increase of temperature and reaction time along non-acidic reactions showed a positive effect on the release of N into process water, because of the hydrolysis of proteins, amino acids, and multi-peptides present in the feedstock [47], allowing obtaining a high nitrogen concentration in PW230 at 30 min (~9.3 g/L, equivalent to 76.5 g/kg C-MBM), and remained constant at the end of the reaction (Fig. 2a). Likewise, HTT-A favored the N solubilization at the lowest reaction temperature (~9.5 g/L, equivalent to 79.5 g/kg C-MBM), because of the positive effect of the acid on the hydrolysis of nitrogenous organic compounds [26]. This effect is consistent with the results obtained by Dai et al. (2017) [48], who reported that N solubilization increased (up to 64% N contained in feedstock) with increasing concentrations of HCl added during HTT, achieving the maximum N release at lower HTT temperature. Similarly, Sarrion et al. (2021) [26] concluded that, under hydrothermal conditions, the most relevant factor on N solubilization of food waste was the acid addition (0.5 M HCl) rather than temperature, achieving almost 100% N solubilization at 170 °C.

The nitrogen speciation (Org-N, NH<sub>4</sub>-N, NO<sub>3</sub>-N and NO<sub>2</sub>-N) in the PW after 60 min reaction time indicated that the concentration of

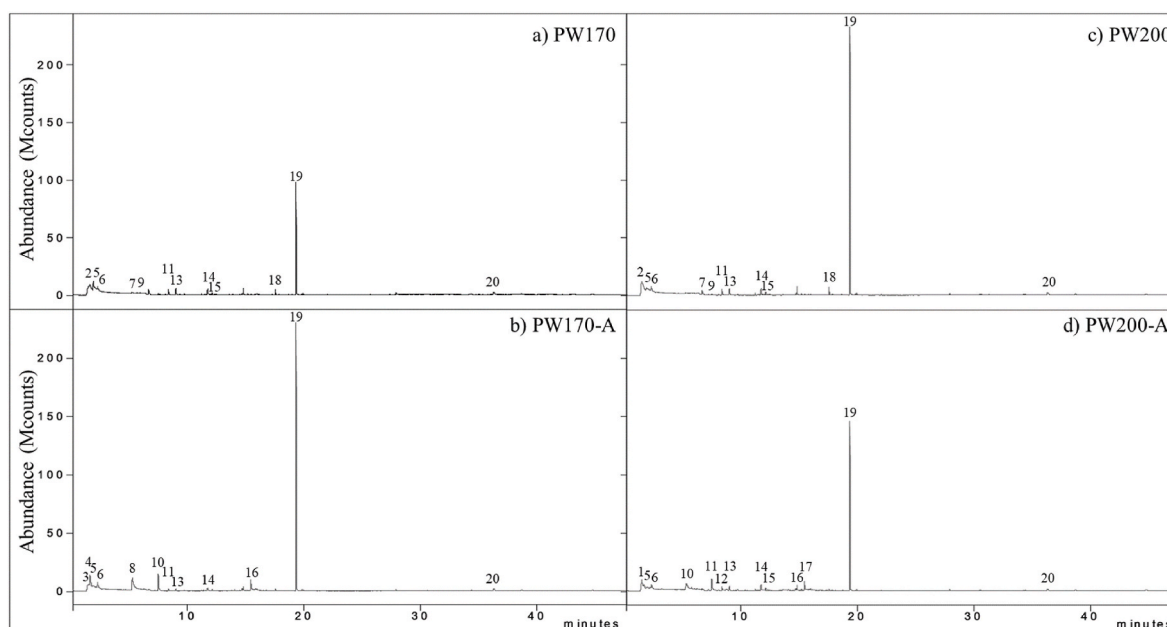


Fig. 4. Organic compounds detected in PW170, PW170-A, PW200, and PW200-A after 60 min reaction time.

**Table 2**

Organic compounds in process water from non-acidic and acid-assisted HTT.

Number	Compound	Peak area			
		PW170	PW170-A	PW200	PW200-A
1	2-Methyl-2-propanamine	–	–	–	7.28·10 <sup>7</sup>
2	Trimethylamine	7.25·10 <sup>7</sup>	–	8.56·10 <sup>7</sup>	–
3	Butane	–	4.96·10 <sup>7</sup>	–	–
4	2,3-Dimethyl pentanal	9.18·10 <sup>7</sup>	9.87·10 <sup>7</sup>	8.68·10 <sup>7</sup>	3.92·10 <sup>7</sup>
5	2-Chloro acetamide	1.46·10 <sup>8</sup>	6.49·10 <sup>7</sup>	9.66·10 <sup>7</sup>	4.34·10 <sup>7</sup>
6	Dimethyl disulfide	7.43·10 <sup>7</sup>	5.25·10 <sup>7</sup>	9.12·10 <sup>7</sup>	4.66·10 <sup>7</sup>
7	Prednisolone acetate	1.57·10 <sup>7</sup>	–	4.27·10 <sup>7</sup>	–
8	Phenyl ester carbamic acid	–	6.97·10 <sup>7</sup>	–	–
9	Ethanethioamide	2.64·10 <sup>7</sup>	–	4.11·10 <sup>7</sup>	–
10	Undecan-1-ol	–	3.90·10 <sup>7</sup>	–	2.54·10 <sup>7</sup>
11	2,3,6-Trichlorobenzaldehyde	1.75·10 <sup>7</sup>	6.06·10 <sup>6</sup>	2.22·10 <sup>7</sup>	1.05·10 <sup>7</sup>
12	Hexadecen-1-ol	–	–	–	6.06·10 <sup>6</sup>
13	N-((7S)-5,6,7,9-tetrahydro-1,2,3,10-tetrametoxi-9-oxobenzo(a)heptalen-7-yl)-acetamida	3.20·10 <sup>7</sup>	1.89·10 <sup>7</sup>	3.43·10 <sup>7</sup>	2.45·10 <sup>7</sup>
14	1,3-Dioxolane	1.42·10 <sup>7</sup>	6.47·10 <sup>6</sup>	1.33·10 <sup>7</sup>	1.27·10 <sup>7</sup>
15	Undecane	5.08·10 <sup>6</sup>	–	7.18·10 <sup>6</sup>	6.23·10 <sup>6</sup>
16	Acetone	–	4.52·10 <sup>7</sup>	–	2.98·10 <sup>7</sup>
17	Ethylparaben	–	–	–	1.02·10 <sup>7</sup>
18	Dexamethasone 2-acetate	9.80·10 <sup>6</sup>	–	1.25·10 <sup>7</sup>	–
19	2,4,6-Trimethoxyacetophenone	1.88·10 <sup>8</sup>	4.43·10 <sup>8</sup>	4.10·10 <sup>8</sup>	2.80·10 <sup>8</sup>
20	t-Butylacetylene	1.35·10 <sup>7</sup>	8.37·10 <sup>6</sup>	1.15·10 <sup>7</sup>	5.53·10 <sup>6</sup>

- relates to the compound was not detected.

detected species was equivalent to the nitrogen contained in the initial feedstock. Org-N was the largest in the process water, decreasing from 71% in PW170 to 61% in PW230, respectively. NH<sub>4</sub>-N increased with the reaction temperature to 30% of the total nitrogen in process water. In all cases, an increase of reaction temperature showed a significant effect on the mineralization of Org-N to NH<sub>4</sub>-N, and this effect was enhanced under acidic conditions. The acid addition in the reaction improved the mineralization of Org-N to NH<sub>4</sub>-N up to 55% of the total nitrogen in process water. The NO<sub>2</sub>-N and NO<sub>3</sub>-N concentration was negligible and accounted <0.1% of the total nitrogen in the process waters.

Fig. 2b shows the time course of phosphorus concentration (as PO<sub>4</sub>-P) in the process water. In the non-acidic HTT, the maximum PO<sub>4</sub>-P concentration (0.35–0.36 g/L, equivalent to 4.0–4.2 g/kg feedstock) reached at 200 and 230 °C after 60 min reaction time, around 30% higher than that obtained at 170 °C. Phosphorous in C-MBM is located in bones as inorganic phosphates, limited its releasing since these compounds are very stable under conventional HTT conditions [15]. Acid-assisted HTT increased up to 10-fold the PO<sub>4</sub>-P solubilization in process water compared with non-acidic conditions.

These values showed a positive effect on the solubilization of PO<sub>4</sub>-P, by action of acid in the reaction promoting the mineralization and solubilization of organic P (mainly contained in proteins and bones) to process water [26,49]. In this way, P contained in bones appears mainly as P-complex with Ca, being both highly soluble elements under acid conditions [48]. As reported Sarrion et al. (2021) [26] and Qaramaleki et al. (2020) [50], HCl-assisted HTT enhanced P solubilization (mainly

as PO<sub>4</sub>-P) from food waste (~94% initially present P in the feedstock) and swine manure (~96% initial P), respectively, compared to conventional HTT tests, achieving a maximum concentration when HCl concentration increased to 0.5 M. In this work, the maximum PO<sub>4</sub>-P concentration is obtained at PW170-A and PW200-A (~3 g/L in both cases). However, increasing the temperature to 230 °C resulted in a decrease in PO<sub>4</sub>-P concentration, around 30% (~1.9 g/L), which suggests that at high temperatures, polymerization reactions are favored, leading to the bonding of P with the solubilized elements, keeping them retained within the bio-oil phase [51]. This decrease in PO<sub>4</sub>-P content together with the energetic cost of increasing the temperature to 230 °C led to discard these process waters (PW230 and PW230-A) to evaluate both nutrient recovery and methane potential.

Fig. 3 shows the distribution of the main mineral elements (Al, Ca, Fe, Mg, Na and K) in the HTT products at 60 min of reaction. Metals such as Al, Fe, Ca and Mg did not suffer leaching to process water during non-acidic HTT and were retained in hydrochar structure [26,52]. Similar trend was observed in ash content (above mentioned) which did not present alteration during HTT process. Monovalent metals, such as Na and K, leached (70% and 85%, respectively) to the process water, while divalent and trivalent metals remain in the hydrochar, mainly due to the formation of insoluble P-complexes under hydrothermal conditions [51].

Acid-assisted HTT promoted the metal leaching to the process water. Monovalent metals were completely lixiviated, while divalent metals (Ca and Mg) were almost dissolved in the process water, highlighting that acid addition improves the degradation of the building components

**Table 3**

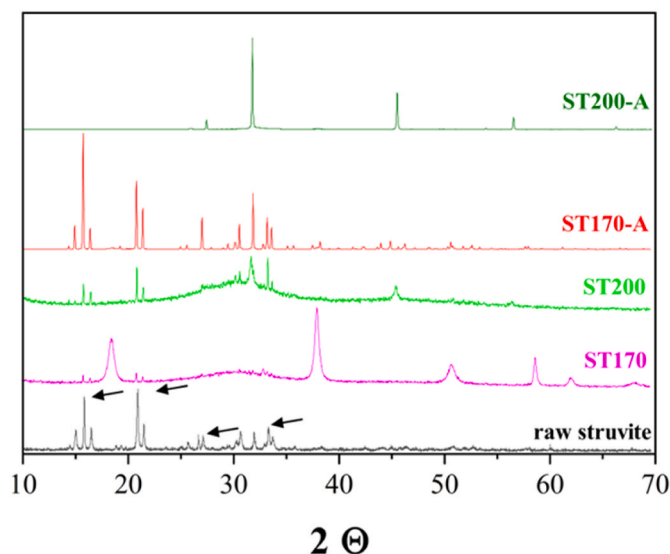
Characterization of process water before and after phosphorous recovery.

	PW170	PW200	PW170-A	PW200-A	PW170-S	PW200-S	PW170-A-S	PW200-A-S
pH	6.5 ± 0.1	6.8 ± 0.1	1.5 ± 0.1	1.8 ± 0.1	8.1 ± 0.1	8.3 ± 0.1	8.1 ± 0.1	8.2 ± 0.1
SCOD (g/L)	75.2 ± 0.6	82.3 ± 0.1	64.3 ± 0.2	61.2 ± 0.4	74.1 ± 0.9	80.5 ± 0.3	64.7 ± 0.6	60.7 ± 1.7
TS (g/L)	63.8 ± 0.7	65.9 ± 0.2	85.5 ± 1.1	81.0 ± 0.8	58.2 ± 1.1	61.0 ± 0.3	79.5 ± 1.0	75.5 ± 0.5
VS (g/L)	55.2 ± 0.8	59.9 ± 0.4	55.2 ± 0.7	51.1 ± 1.0	52.3 ± 1.8	56.0 ± 0.0	50.7 ± 1.0	47.6 ± 1.4
TKN (g/L)	8.7 ± 0.1	9.0 ± 0.1	9.6 ± 0.1	9.5 ± 0.1	8.1 ± 0.2	7.4 ± 0.2	8.7 ± 0.1	7.6 ± 0.1
Org-N (g/L)	7.7 ± 0.1	7.0 ± 0.1	8.0 ± 0.1	7.1 ± 0.1	7.5 ± 0.2	6.8 ± 0.2	8.3 ± 0.2	7.0 ± 0.1
NH <sub>4</sub> -N (g/L)	1.0 ± 0.1	1.9 ± 0.1	1.5 ± 0.1	2.3 ± 0.1	0.6 ± 0.0	0.6 ± 0.1	0.4 ± 0.0	0.6 ± 0.0
NO <sub>3</sub> -N (g/L)	0.03 ± 0.0	0.05 ± 0.0	0.05 ± 0.0	0.06 ± 0.0	0.02 ± 0.0	0.05 ± 0.0	0.05 ± 0.0	0.05 ± 0.0
NO <sub>2</sub> -N (g/L)	<0.01 ± 0.0	<0.01 ± 0.0	<0.01 ± 0.0	<0.01 ± 0.0	<0.01 ± 0.0	<0.01 ± 0.0	<0.01 ± 0.0	<0.01 ± 0.0
PO <sub>4</sub> -P (g/L)	0.3 ± 1.6	0.4 ± 1.2	3.0 ± 1.2	3.0 ± 1.3	<0.1 ± 0.0	<0.1 ± 0.0	1.0 ± 0.2	0.5 ± 0.1
Ca (g/L)	0.7 ± 0.0	0.3 ± 0.0	3.5 ± 0.1	3.9 ± 0.1	<0.1 ± 0.0	<0.1 ± 0.0	0.1 ± 0.0	0.1 ± 0.0
Mg (g/L)	<0.1 ± 0.0	<0.1 ± 0.0	0.1 ± 0.0	0.4 ± 0.0	<0.1 ± 0.0	<0.1 ± 0.0	4.3 ± 0.2	1.5 ± 0.1

**Table 4**

Mineral and heavy metal content of struvite-like solids.

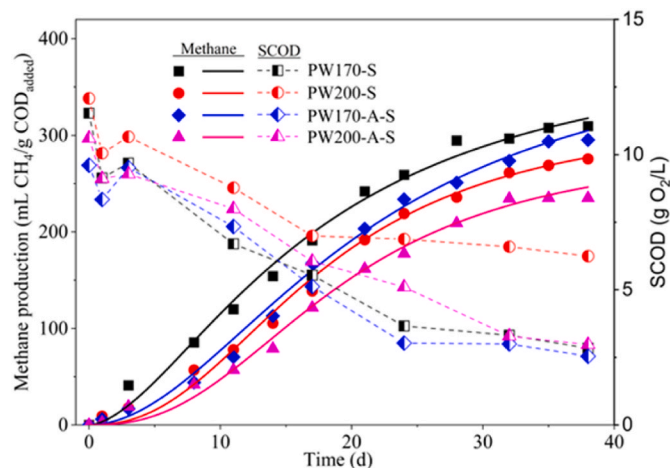
Mineral metals (g/kg)	ST170	ST200	ST170-A	ST200-A
Na	5.0	0.8	2.6	13.6
Ca	70.9	1.5	4.3	117
K	1.3	4.4	4.7	2.7
Mg	157	147	100	14.6
P	72.0	189	126	132
Heavy metals (mg/kg)				
Cd	0.1	0.1	<0.01	0.1
Cr	10.6	14.7	4.3	33.4
Cu	5.6	0.4	0.8	1.0
Ni	17.1	1.2	1.3	2.6
Pb	5.3	2.8	0.8	2.5
Zn	659	214	19.4	253

**Fig. 5.** X-ray diffractogram and nutrients content of struvite-like solids.

of the bones structure to the process water (see Table 1 and Fig. 3).

Fig. 4 and Table 2 show the main organic compounds in PW and PW-A at 170 and 200 °C. The increase of temperature reduced the presence of short chain organic compounds and increased the amount of long chain compound (e.g. 2,3-dimethyl pentanal) and aromatic species (e.g. 1,3-dioxolane). It is associated with the reaction pathways during conventional HTT, which include hydrolysis, dehydration, decarboxylation, condensation, polymerization, and aromatization reactions [29]. Furthermore, the compounds identified were similar to those observed in process waters from the HTC of cellulose and carbohydrates [53,54]. In the case of PW-A, long chain compounds and aromatic species decreased or were totally removed, indicating that the addition of acid favored their hydrolysis into short-chain compounds. Other compounds such as amines (e.g. trimethylamine), steres (e.g. phenyl ester carbamic acid), and sulphides (e.g. dimethyl disulphide) detected in acid-free process water were substantially removed or hydrolyzed in PW-A. Amine degradation under acidic conditions is associated with an increase in the  $\text{NH}_4\text{-N}$  content in PW-A.

Likewise, compounds such as aldehydes, alcohols, or acetone, not detected in process water from non-acidic HTT, appears in process water from acid-assisted HTT. Noteworthy that complex compounds related to drugs or antibiotics used in animal husbandry (prednisolone acetate, dexamethasone 2-acetate) were detected in process water from conventional HTT but were not detected in process water from acidic HTT (Fig. 4) probably due to the severity of HTT process at acidic conditions.

**Fig. 6.** Methane production and SCOD removal. Symbols represent experimental values and solid lines indicate theoretical values (first-order equation) for methane production. Symbols and dash lines correspond to experimental SCOD time course.

### 3.3. Phosphorous and nitrogen recovery from process water

Process water from non-acidic and acid-assisted HTT were characterized before and after nutrient recovery stage. Table 3 collects the main characteristics of process waters (PW, PW-A, PW-S and PW-A-S). Acid-free PW and PW-A obtained at 230 °C were discarded for presenting the lowest P concentration.

As expected, the PW-A presents low pH (<2), while acid-free PW shows close to neutral pH ( $\approx 7$ ). This pH difference has a remarkable impact on the solubilization of metals. The solubility product of metals increases at acidic pH values, which has already been observed in the distribution of nutrients and metals (see Figs. 2 and 3). The content of Ca, Mg and P in PW-A was remarkably higher than in acid-free PW (Table 3). Likewise, the nitrogen content (TKN and  $\text{NH}_4\text{-N}$ ) was slightly high in PW-A than in acid-free PW, with a minimum contribution of  $\text{NO}_3\text{-N}$  and  $\text{NO}_2\text{-N}$  (being <0.1 g/L in all cases, which represents less than 1% of total dissolved nitrogen).

PW and PW-A, except those obtained at 230 °C as previously mentioned were subjected to nutrient recovery to produce struvite. After nutrient recovery stage the phosphorus and nitrogen content were reduced up to 95 and 51%, respectively. In addition, Ca and Mg content was almost removed in PW-S, which also affects the TS content, reduced on average around 10%. The nitrogen content (TKN and  $\text{NH}_4\text{-N}$ ) also decreased, mainly due to the removal of  $\text{NH}_4\text{-N}$  (which participated in the formation of struvite;  $(\text{NH}_4)\text{MgPO}_4 \cdot 6\text{H}_2\text{O}$ ), while the Org-N remained unchanged.

Table 4 and Fig. 5 show the mineral and heavy metals content and diffraction patterns of solid precipitates. Although the solids recovered from PW170 and PW200 (ST170 and ST200) were rich in P and Mg, the crystalline structure of these materials did not present a defined shape. The amorphous shape of ST170 and ST200 was probably caused by the high concentration of Ca ( $\approx 71$  and 106 g/kg, respectively), which could indicate the formation of calcium phosphate salts, such as apatite or hydroxyapatite instead of struvite [55]. Similar results were observed for ST200-A, where the peaks resembled apatite more than struvite [56], which is corroborated by the higher Ca than Mg content. On other hand, the structure of ST170-A presented clear crystalline peaks similar to pure struvite [56] and higher content of  $\text{PO}_4\text{-P}$  (126 g/kg) and Mg (100 g/kg). The N/P/K content of the solids was in the range of 1.3–2.3/7.2–12.6/0.1–0.5. However, the recovery yield of ST170-A and ST200-A (201–204 g solid per kg dry C-MBM) was more interesting compared to that of ST170 and ST200 (20–23 g solid per kg dry C-MBM). Additionally, the nutrient recovery step did not result in a precipitate

**Table 5**

Experimental ( $G_e$ ) and theoretical ( $G_t$ ) ultimate methane yield and fitting parameters.

	PW170-S	PW200-S	PW170-A-S	PW200-A-S
$G_e$ (mL CH <sub>4</sub> /g COD <sub>added</sub> )	300 ± 3	235 ± 3	275 ± 5	266 ± 4
$G_t$ (mL CH <sub>4</sub> /g COD <sub>added</sub> )	322 ± 14	241 ± 8	302 ± 13	283 ± 8
$k$ (d <sup>-1</sup> )	0.059 ± 0.01	0.050 ± 0.01	0.048 ± 0.01	0.051 ± 0.01
$R^2$	0.999	0.997	0.992	0.999
COD removal (%)	75.3	42.2	62.2	71.9

with a high organic matter (ranging from 1.8 to 2.6% in all cases) and heavy metal content. The heavy metals content in the precipitated solids showed values below those established in the Regulation (EU) 2019/1009 [57], for the use of mineral fertilizers on agricultural soils.

### 3.4. Anaerobic digestion of secondary process water

Fig. 6 shows the SCOD removal and methane production along anaerobic digestion of PW170-S, PW200-S, PW170-A-S, and PW200-A-S. A rapid decrease in SCOD (15–20%) and an increase of methane production (85–150 mL STP CH<sub>4</sub>/g COD<sub>added</sub>), related to easily assimilated soluble compounds, mainly as acetate (650 mg COD/L), were observed in the first days. The methane production was around 250–305 mL STP CH<sub>4</sub>/g COD<sub>added</sub> with a SCOD removal between 50 and 75%. According to these values, the increase in temperature and the acidic HTT conditions showed a detrimental effect on the methanogenic microorganisms, reflected in the lower methane production and organic matter removal. Furthermore, the increase in temperature played a more outstanding role than the addition of acid, since the highest methane production and the organic matter removal were determined in the process water obtained at the lowest temperature tested.

The experimental methane production fitted adequately to a first-order kinetic model (Fig. 6, Table 5) since no lag phase was observed at the beginning of the test, which indicates that it is a substrate with a high content of biodegradable organic matter. The low presence of recalcitrant compounds is associated with the negligible carbohydrate content as well as the high protein and fat content of C-MBM. According to Yang et al. [58] recalcitrant compounds are generally formed by Maillard reactions between an amino acid and a carbohydrate, which due to the nature of C-MBM discourages the formation of recalcitrant compounds that usually inhibit methanogenic microorganisms. This is evidenced by the analysis of the diversity of organic compounds in the process water (see Table 2 and Fig. 4). The process water is rich in alkyl compounds and has a low content of aromatic compounds. The kinetic constant ( $k$ ) was in the range of 0.05–0.059 d<sup>-1</sup>, while Mannarino et al. (2021) obtained 0.105 d<sup>-1</sup> from process water of food waste composed mainly of fruits and vegetables [59]. Considering the theoretical methane production and the high organic matter content of the process water, around 20–23 L CH<sub>4</sub> STP/kg C-MBM were obtained.

## 4. Conclusions

Hydrothermal treatment is presented as a potential technology to valorize meat and poultry bone meal waste. Conventional HTT produced a hydrochar with poor characteristics to be used as biofuel, while acid-assisted HTT yielded a bio-oil with high HHV and suitable characteristics to be used as an alternative biofuel. Acid-assisted HTT almost completely promoted the solubilization of phosphorus, calcium, magnesium, and nitrogen in the process water. The solid precipitated by addition of a Mg salt showed a crystalline structure in a struvite-apatite mixture. Anaerobic digestion of the process water allowed removal of up to 75% organic matter and high methane production (250–305 CH<sub>4</sub> STP/g COD<sub>added</sub>) with a better performance for process water obtained

at 170 °C. The treatment of chicken meat and bone meal waste by HTT represents a new management pathway for material and energy valorization in a circular economy framework.

## Declaration of competing interest

The authors declare that they have no known competing financial interests or personal relationships that could have appeared to influence the work reported in this paper.

## Data availability

Data will be made available on request.

## Acknowledgements

Authors greatly appreciate funding from Spain's MINECO (PID2019-108445RB-I00, PDC2021-120755-I00), Madrid Regional Government (Project S2018/EMT-4344) and Grupo Kerbest Company. A. Sarrion wishes to thank the Spanish MICINN and ESF for a research grant (BES-2017-081515). R.P. Ipiales acknowledges financial support from Community of Madrid (IND2019/AMB-17092) and Arquimea-Agrotech Company.

## References

- [1] T.M. Hicks, C.J.R. Verbeek, in: G.B.T.-P.B. Singh Dhillon (Ed.), Chapter 3-Meat Industry Protein By-Products: Sources and Characteristics, Academic Press, 2016, pp. 37–61, <https://doi.org/10.1016/B978-0-12-802391-4.00003-3>.
- [2] F.J. Andriamanohiarisoamanana, A. Saikawa, T. Kan, G. Qi, Z. Pan, T. Yamashiro, M. Iwasaki, I. Ihara, T. Nishida, K. Umetsu, Semi-continuous anaerobic co-digestion of dairy manure, meat and bone meal and crude glycerol: process performance and digestate valorization, *Renew. Energy* 128 (2018) 1–8, <https://doi.org/10.1016/j.renene.2018.05.056>.
- [3] G. Wu, M.G. Healy, X. Zhan, Effect of the solid content on anaerobic digestion of meat and bone meal, *Bioresour. Technol.* 100 (2009) 4326–4331, <https://doi.org/10.1016/j.biortech.2009.04.007>.
- [4] M. Kantorek, K. Jesionek, S. Polesek-Karczewska, P. Ziolkowski, M. Stajnke, J. Badur, Thermal utilization of meat-and-bone meal using the rotary kiln pyrolyzer and the fluidized bed boiler – the performance of pilot-scale installation, *Renew. Energy* 164 (2021) 1447–1456, <https://doi.org/10.1016/J.RENENE.2020.10.124>.
- [5] F.J. Andriamanohiarisoamanana, A. Saikawa, K. Tarukawa, G. Qi, Z. Pan, T. Yamashiro, M. Iwasaki, I. Ihara, T. Nishida, K. Umetsu, Anaerobic co-digestion of dairy manure, meat and bone meal, and crude glycerol under mesophilic conditions: synergistic effect and kinetic studies, *Energy Sustain. Dev.* 40 (2017) 11–18, <https://doi.org/10.1016/j.esd.2017.05.008>.
- [6] W.K.H. Ariyaratne, M.C. Melaen, K. Eine, L.A. Tokheim, Meat and bone meal as a renewable energy source in cement kilns: investigation of optimum feeding rate, *Renew. Energy Power Qual. J.* 1 (2011) 1244–1249, <https://doi.org/10.24084/repqj09.609>.
- [7] S.N. Misi, C.F. Forster, Batch co-digestion of multi-component agro-wastes, *Bioresour. Technol.* 80 (2001) 19–28, [https://doi.org/10.1016/S0960-8524\(01\)00078-5](https://doi.org/10.1016/S0960-8524(01)00078-5).
- [8] A. Magdziarz, M. Gajek, D. Nowak-Woźny, M. Wilk, Mineral phase transformation of biomass ashes—Experimental and thermochemical calculations, *Renew. Energy* 128 (2018) 446–459, <https://doi.org/10.1016/j.renene.2017.05.057>.
- [9] L. Fryda, K. Panopoulos, P. Vourliotis, E. Kakaras, E. Pavlidou, Meat and bone meal as secondary fuel in fluidized bed combustion, *Proc. Combust. Inst.* 31 (2007) 2829–2837, <https://doi.org/10.1016/J.PROCI.2006.07.151>.
- [10] N. Krishnamoorthy, B. Dey, Y. Unpaprom, R. Ramaraj, G.P. Maniam, N. Govindan, S. Jayaraman, T. Arunachalam, B. Paramasivan, Engineering principles and process designs for phosphorus recovery as struvite: a comprehensive review, *J. Environ. Chem. Eng.* 9 (2021), 105579, <https://doi.org/10.1016/J.JECE.2021.105579>.
- [11] European Commission, On the Review of the List of Critical Raw Materials for the EU and the Implementation of the Raw Materials Initiative, Off. J. Eur. Union, 2014. COM(2014) 297 final.
- [12] L. Leng, L. Yang, S. Leng, W. Zhang, Y. Zhou, H. Peng, H. Li, Y. Hu, S. Jiang, H. Li, A review on nitrogen transformation in hydrochar during hydrothermal carbonization of biomass containing nitrogen, *Sci. Total Environ.* 756 (2021), 143679, <https://doi.org/10.1016/J.SCITOTENV.2020.143679>.
- [13] Eurostat, Waste Statistics, 2021. [https://ec.europa.eu/eurostat/statistics-explained/index.php?title=Waste\\_statistics](https://ec.europa.eu/eurostat/statistics-explained/index.php?title=Waste_statistics).
- [14] Eurostat, Mineral Fertiliser Consumption in EU, 2020. <https://ec.europa.eu/eurostat/web/products-eurostat-news/-/ddn-20220628-1#:text=The amount of mineral fertilisers,8.3%25 increase compared with 2010.>
- [15] L. Leng, J. Zhang, S. Xu, Q. Xiong, X. Xu, J. Li, H. Huang, Meat & bone meal (MBM) incineration ash for phosphate removal from wastewater and afterward



- phosphorus recovery, *J. Clean. Prod.* 238 (2019), 117960, <https://doi.org/10.1016/J.JCLEPRO.2019.117960>.
- [16] R.P. Ipiales, M.A. de la Rubia, E. Diaz, A.F. Mohedano, J.J. Rodriguez, Integration of hydrothermal carbonization and anaerobic digestion for energy recovery of biomass waste: an overview, *Energy Fuel*. 35 (2021) 17032–17050, <https://doi.org/10.1021/acs.energyfuels.1c01681>.
- [17] A. Kruse, A. Funke, M.M. Titirici, Hydrothermal conversion of biomass to fuels and energetic materials, *Curr. Opin. Chem. Biol.* 17 (2013) 515–521, <https://doi.org/10.1016/j.cbpa.2013.05.004>.
- [18] D. Gupta, S.M. Mahajani, A. Garg, Effect of hydrothermal carbonization as pretreatment on energy recovery from food and paper wastes, *Bioresour. Technol.* 285 (2019), 121329, <https://doi.org/10.1016/j.biortech.2019.121329>.
- [19] K.S. Ro, J.A. Libra, S. Bae, N.D. Berge, J.R.V. Flora, R. Pecenk, Combustion behavior of animal-manure-based hydrochar and pyrochar, *ACS Sustain. Chem. Eng.* 7 (2019) 470–478, <https://doi.org/10.1021/ACSSUSCHEMENG.8B03926>.
- [20] A. Khosravi, H. Zheng, Q. Liu, M. Hashemi, Y. Tang, B. Xing, Production and characterization of hydrochars and their application in soil improvement and environmental remediation, *Chem. Eng. J.* 430 (2022), 133142, <https://doi.org/10.1016/J.CEJ.2021.133142>.
- [21] P.J. Arauzo, P.A. Maziarka, K.A. Schoder, J. Pfersich, F. Ronsse, A. Kruse, Influence of sequential HTC pre-treatment and pyrolysis on wet food-industry wastes: optimisation toward nitrogen-rich hierarchical carbonaceous materials intended for use in energy storage solutions, *Sci. Total Environ.* 816 (2022), 151648, <https://doi.org/10.1016/J.SCITOTENV.2021.151648>.
- [22] J.A. Villamil, E. Diaz, M.A. de la Rubia, A.F. Mohedano, Potential use of waste activated sludge hydrothermally treated as a renewable fuel or activated carbon precursor, *Mol* 25 (2020), <https://doi.org/10.3390/MOLECULES25153534>, 3534, 25 (2020) 3534.
- [23] A.S. Oliveira, J.A. Baeza, L. Calvo, N. Alonso-Morales, F. Heras, J.J. Rodriguez, M. A. Gilarranz, Production of hydrogen from brewery wastewater by aqueous phase reforming with Pt/C catalysts, *Appl. Catal. B Environ.* 245 (2019) 367–375, <https://doi.org/10.1016/j.apcatb.2018.12.061>.
- [24] C.I. Aragón-Briceño, A.K. Pozarlik, E.A. Bramer, L. Niedzwiecki, H. Pawlak-Kruczek, G. Brem, Hydrothermal carbonization of wet biomass from nitrogen and phosphorus approach: a review, *Renew. Energy* 171 (2021) 401–415, <https://doi.org/10.1016/j.renene.2021.02.109>.
- [25] R.P. Ipiales, A.F. Mohedano, E. Diaz, M.A. de la Rubia, Energy recovery from garden and park waste by hydrothermal carbonisation and anaerobic digestion, *Waste Manag.* 140 (2022) 100–109, <https://doi.org/10.1016/j.wasman.2022.01.003>.
- [26] A. Sarrion, E. Diaz, M. Angeles de la Rubia, A.F. Mohedano, Fate of nutrients during hydrothermal treatment of food waste, *Bioresour. Technol.* (2021), 125954, <https://doi.org/10.1016/j.biortech.2021.125954>.
- [27] G.C. Becker, D. Wüst, H. Köhler, A. Lautenbach, A. Kruse, Novel approach of phosphate-reclamation as struvite from sewage sludge by utilising hydrothermal carbonization, *J. Environ. Manag.* 238 (2019) 119–125, <https://doi.org/10.1016/j.jenvman.2019.02.121>.
- [28] A. Weideler, J. Krampe, H. Steinmetz, Phosphorrückgewinnung aus kommunalem Klärschlamm als Magnesium-Ammonium-Phosphat (MAP), *Wasser Und Abfall*, 2008, pp. 23–26.
- [29] J.A. Villamil, A.F. Mohedano, J.J. Rodriguez, M.A. De la Rubia, Valorisation of the liquid fraction from hydrothermal carbonisation of sewage sludge by anaerobic digestion, *J. Chem. Technol. Biotechnol.* 93 (2017) 450–456, <https://doi.org/10.1002/jctb.5375>.
- [30] ASTM, Standard Test Methods for Proximate Analysis of Coal and Coke by Macro Thermogravimetric Analysis, ASTM-International, Pennsylvania, 2015. Method D7582-15.
- [31] S.A. Channiwal, P.P. Parikh, A unified correlation for estimating HHV of solid, liquid and gaseous fuels, *Fuel* 81 (2002) 1051–1063, [https://doi.org/10.1016/S0016-2361\(01\)00131-4](https://doi.org/10.1016/S0016-2361(01)00131-4).
- [32] APHA, Standard Methods for the Examination of Water and Wastewater, twenty-first ed., American Public Health Association, Washington, DC., USA, 2005.
- [33] F. Raposo, M.A. de la Rubia, R. Borja, M. Alaiz, Assessment of a modified and optimised method for determining chemical oxygen demand of solid substrates and solutions with high suspended solid content, *Talanta* 76 (2008) 448–453, <https://doi.org/10.1016/j.talanta.2008.03.030>.
- [34] M.A. De la Rubia, J.A. Villamil, J.J. Rodriguez, R. Borja, A.F. Mohedano, Mesophilic anaerobic co-digestion of the organic fraction of municipal solid waste with the liquid fraction from hydrothermal carbonization of sewage sludge, *Waste Manag.* 76 (2018) 315–322, <https://doi.org/10.1016/j.wasman.2018.02.046>.
- [35] M.A. De la Rubia, J.A. Villamil, J.J. Rodriguez, A.F. Mohedano, Effect of inoculum source and initial concentration on the anaerobic digestion of the liquid fraction from hydrothermal carbonisation of sewage sludge, *Renew. Energy* 127 (2018) 697–704, <https://doi.org/10.1016/j.renene.2018.05.002>.
- [36] Q. Lang, B. Zhang, Z. Liu, Z. Chen, Y. Xia, D. Li, J. Ma, C. Gai, Co-hydrothermal carbonization of corn stalk and swine manure: combustion behavior of hydrochar by thermogravimetric analysis, *Bioresour. Technol.* 271 (2019) 75–83, <https://doi.org/10.1016/j.biortech.2018.09.100>.
- [37] A.A. Khan, W. de Jong, P.J. Jansens, H. Spliethoff, Biomass combustion in fluidized bed boilers: potential problems and remedies, *Fuel Process. Technol.* 90 (2009) 21–50, <https://doi.org/10.1016/j.fuproc.2008.07.012>.
- [38] M. Ayllón, G. Gea, M.B. Murillo, J.L. Sánchez, J. Arauzo, Kinetic study of meat and bone meal pyrolysis: an evaluation and comparison of different possible kinetic models, *J. Anal. Appl. Pyrolysis* 74 (2005) 445–453, <https://doi.org/10.1016/j.jaap.2004.11.022>.
- [39] M. Lucian, M. Volpe, L. Gao, G. Piro, J.L. Goldfarb, L. Fiori, Impact of hydrothermal carbonization conditions on the formation of hydrochars and secondary chars from the organic fraction of municipal solid waste, *Fuel* 233 (2018) 257–268, <https://doi.org/10.1016/j.fuel.2018.06.060>.
- [40] S. Román, J. Libra, N. Berge, E. Sabio, K. Ro, L. Li, B. Ledesma, A. Alvarez, S. Bae, Hydrothermal carbonization: modeling, final properties design and applications: a review, *Energies* 11 (2018) 1–28, <https://doi.org/10.3390/en11010216>.
- [41] E. Cascarosa, G. Gea, J. Arauzo, Thermochemical processing of meat and bone meal: a review, *Renew. Sustain. Energy Rev.* 16 (2012) 942–957, <https://doi.org/10.1016/j.rser.2011.09.015>.
- [42] ISO/TS 17225-8, International Organization for Standardization ISO/TS 17225-8. Solid Biofuels — Fuel Specifications and Classes. Graded Thermally Treated and Densified Biomass Fuels, first ed., 2016. USA.
- [43] T. Wang, Y. Li, D. Zhi, Y. Lin, K. He, B. Liu, H. Mao, Assessment of combustion and emission behavior of corn straw biochar briquette fuels under different temperatures, *J. Environ. Manag.* 250 (2019), 109399, <https://doi.org/10.1016/j.jenvman.2019.109399>.
- [44] W. Abdelmoez, T. Nakahashi, H. Yoshida, Amino acid transformation and decomposition in saturated subcritical water conditions, *Ind. Eng. Chem. Res.* 46 (2007) 5286–5294.
- [45] N. Sato, A.T. Quitain, K. Kang, H. Daimon, K. Fujie, Reaction kinetics of amino acid decomposition in high-temperature and high-pressure water, *Ind. Eng. Chem. Res.* 43 (2004) 3217–3222, <https://doi.org/10.1021/ie020733n>.
- [46] H. Ahn, D. Kim, Y. Lee, Combustion characteristics of sewage sludge solid fuels produced by drying and hydrothermal carbonization in a fluidized bed, *Renew. Energy* 147 (2020) 957–968, <https://doi.org/10.1016/j.renene.2019.09.057>.
- [47] A. Kruse, F. Koch, K. Stelzl, D. Wüst, M. Zeller, Fate of nitrogen during hydrothermal carbonization, *Energy Fuel*. 30 (2016) 8037–8042, <https://doi.org/10.1021/acs.energyfuels.6b01312>.
- [48] L. Dai, B. Yang, H. Li, F. Tan, N. Zhu, Q. Zhu, M. He, Y. Ran, G. Hu, A synergistic combination of nutrient reclamation from manure and resultant hydrochar upgradation by acid-supported hydrothermal carbonization, *Bioresour. Technol.* 243 (2017) 860–866, <https://doi.org/10.1016/j.biortech.2017.07.016>.
- [49] T. Zhang, X. He, Y. Deng, D.C.W. Tsang, R. Jiang, G.C. Becker, A. Kruse, Phosphorus recovered from digestate by hydrothermal processes with struvite crystallization and its potential as a fertilizer, *Sci. Total Environ.* 698 (2020), 134240, <https://doi.org/10.1016/J.SCITOTENV.2019.134240>.
- [50] S.V. Qaramaleki, J.A. Villamil, A.F. Mohedano, C.J. Coronella, Factors affecting solubilization of phosphorus and nitrogen through hydrothermal carbonization of animal manure, *ACS Sustain. Chem. Eng.* 8 (2020) 12462–12470, <https://doi.org/10.1021/acssuschemeng.0c03268>.
- [51] A. Sarrion, A. de la Rubia, C. Coronella, A.F. Mohedano, E. Diaz, Acid-mediated hydrothermal treatment of sewage sludge for nutrient recovery, *Sci. Total Environ.* 838 (2022), 156494, <https://doi.org/10.1016/j.scitotenv.2022.156494>.
- [52] M.T. Reza, J.G. Lynam, M.H. Uddin, C.J. Coronella, Hydrothermal carbonization : fate of inorganics, *Biomass Bioenergy* 49 (2013) 86–94, <https://doi.org/10.1016/j.biombioe.2012.12.004>.
- [53] E. García-Bordejé, E. Pires, J.M. Fraile, Parametric study of the hydrothermal carbonization of cellulose and effect of acidic conditions, *Carbon N. Y.* 123 (2017) 421–432, <https://doi.org/10.1016/j.carbon.2017.07.085>.
- [54] J. Poerschmann, B. Weiner, R. Koehler, F.D. Kopinke, Hydrothermal carbonization of glucose, fructose, and xylose - identification of organic products with medium molecular masses, *ACS Sustain. Chem. Eng.* 5 (2017) 6420–6428, <https://doi.org/10.1021/acssuschemeng.7b00276>.
- [55] X. Liu, J. Wang, Impact of calcium on struvite crystallization in the wastewater and its competition with magnesium, *Chem. Eng. J.* 378 (2019), 122121, <https://doi.org/10.1016/j.cej.2019.122121>.
- [56] H.-C. Chang, P.-Y. Chou, M.-P. Cheng, T.-H. Hsiao, K.-Y. Lo, S.-L. Wang, Phosphorus conversion during anaerobic digestion of high-calcium chicken manures and phosphorus recovery as struvite, *J. Environ. Chem. Eng.* 10 (2022), 107615, <https://doi.org/10.1016/j.jece.2022.107615>.
- [57] European Commission, Regulation EU 2019/1009, of, *Off. J. Eur. Union* 129 (2022) 1–125.
- [58] G. Yang, H. Liu, Y. Li, Q. Zhou, M. Jin, H. Xiao, H. Yao, Kinetics of hydrothermal carbonization of kitchen waste based on multi-component reaction mechanism, *Fuel* 324 (2022), 124693, <https://doi.org/10.1016/j.fuel.2022.124693>.
- [59] G. Mannarino, A. Sarrion, E. Diaz, R. Gori, M.A. De la Rubia, A.F. Mohedano, Improved energy recovery from food waste through hydrothermal carbonization and anaerobic digestion, *Waste Manag.* 142 (2022) 9–18, <https://doi.org/10.1016/J.WASMAN.2022.02.003>.